Investigation of scatter from out of the field of view and multiple scatter in PET using Monte Carlo simulations*

YE Ting(叶婷)[1,2] CHAI Pei(柴培)[1] GAO Juan(高娟)[1,2] YUN Ming-Kai(员明凯)[1]
LIU Shuang-Quan(刘双全)[1,2] SHAN Bao-Ci(单保慈)[1;1)] WEI Long(魏龙)[1]

[1] Key Laboratory of Nuclear Analysis Techniques, Institute of High Energy Physics, Chinese Academy of Sciences, Beijing 100049, China
[2] Graduate University of Chinese Academy of Sciences, Beijing 100049, China

Abstract: In fully three-dimensional (3D) positron emission tomography (PET) imaging, the scatter fraction (SF) is about 40%–60%, which may degrade the imaging quality severely. Scatter correction is important for high quality image reconstruction. Model-based scatter correction has been proved to be accurate and available in clinical PET. However, it does not correct the scatter from out of the field of view (OFOV) and multiple scatters. In this study, we demonstrate the radial and axial distribution of scatters from OFOV when the source is located in different radial positions. In order to apply the above conclusions to different PET systems, we characterize the scatters from OFOV as a function of the ratio of the scanner diameter to the length of the axial field of view (AFOV) by modeling several typical whole-body and micro PET systems. The proportions of true events (S_{0-0}), single scatter of one photon (S_{1-0}), single scatter of both photons (S_{1-1}), double scatter of one photon (S_{2-0}) and multiple scatter ($S_{\rm m}$) are also calculated and compared. Here the 3D-PET Monte Carlo simulations are performed with the Geant4 Application for Tomography Emission (GATE). In summary, the scatters from OFOV tend to be recorded on the lines of response (LOR) far away from the source. They have a much more serious impact on whole-body PET than micro PET depending on the ratio of scanner diameter to the length of AFOV. In whole-body PET, twice scatters including single scatter of both photons (S_{1-1}) and double scatter of one photon (S_{2-0}) add up to about 12% so that twice scatter correction must be taken into account to acquire a high quality reconstruction image.

Key words: PET, Monte Carlo simulation, GATE, scattering

PACS: 87.55.k-, 87.57.uk, 87.57.C- **DOI:** 10.1088/1674-1137/35/12/017

1 Introduction

In three-dimensional (3D) positron emission tomography (PET), the allowance of acquisition of all the oblique planes increases the sensitivity, while scatter events increase significantly, which may degrade the imaging quality severely. The proportion of scatter events is referred to as the scatter fraction (SF) and its magnitude depends on the object size and density of the scattering medium, the PET scanner geometry and the width of the energy window. The SF typically reaches 40%–60% in the 3D PET [1]. Therefore, scatter correction is important for high quality image reconstruction.

The single scatter simulation (SSS) algorithm was first proposed by Ollinger and Watson. It has been proved to be one of the most accurate scatter correction methods. In the SSS algorithm, the scatter coincidence probability is calculated assuming that only one of the annihilation photons undergoes once Compton interaction [2, 3]. However, the difficulty in SSS correction is that it does not correct considerable scatter contributions from matter and activity out of the field of view (OFOV) and multiple scatter events for quantitative analysis. In previous studies, efforts were made to achieve many effective results to characterize the scatters from OFOV and multiple scatters and correct them using the Monte Carlo si-

Received 14 February 2011, Revised 8 March 2011
* Supported by National High Technology Research and Development Program of China (863) (2006AA020803), Major State Basic Research Development Program (973) (2007CB512303) and National Natural Science Foundation of China (81101070)
1) E-mail: shanbc@ihep.ac.cn

mulation. Ollinger convoluted the single scatter distribution with a Gaussian kernel for multiple scatter distribution and used several bed positions to account for the activity from OFOV [2]. Adam et al. moved a point source from the center of the axial field of view (AFOV) to OFOV in a water-filled cylinder and concluded that the activity from OFOV had to be taken into consideration for an accurate scatter correction and the multiple scatter had a different spatial distribution from a single scatter [4]. Lewellen et al. performed a series of simulations with a point source to show single and multiple scatter distributions from matter and activity OFOV in 3D PET. They also noted that the spatial scatter distributions from external matter and external activity were different [5]. Gao et al. fitted the axial distribution of scatters from OFOV with a quadratic curve and multiple scatter as a linear function of the object transverse area, respectively [6].

In this paper, we will demonstrate the distribution of scatters from OFOV when the line source is located in different radial positions, which has not been reported yet as far as we know. In order to apply all the conclusions to different PET systems, we characterize the scatters from OFOV and multiple scatters by modeling several typical whole-body and micro PET systems. The fraction of scatters from OFOV (OFOV SF) as a function of ratio of scanner diameter to the length of AFOV is provided first. We also calculate the proportions of true events (S_{0-0}), single scatter of one photon (S_{1-0}), single scatter of both photons (S_{1-1}), double scatter of one photon (S_{2-0}) and multiple scatter (S_{m}), and quantified the influence of multiple scatters between the whole-body PET and the micro PET, which few studies have accessed before. The software used for the simulations here is the Geant4 Application for Tomography Emission (GATE), which is a powerful research tool developed for nuclear medicine imaging applications [7, 8]. The validation of GATE for the simulation of different whole-body and micro PET systems has been well studied [9–11]. These results are useful for the SSS algorithm in particular.

2 Methods

The GATE simulation platform has the capability to precisely and effectively model all physics phenomena, complex scanner geometry, and phantom and source distribution. It offers specific information of each coincidence event, including the scattering times of each photon [12, 13]. In this work, the photoelectric effect and Compton scattering were taken into account. All simulated experiments have a coincidence timing window of 6 ns, an energy resolution of 12% and an energy window of 350 to 650 keV. According to the NEMA protocol [14] and IEC protocol [15], we designed the proper simulation time to obtain enough event counts. In our simulations, coincidences were collected to ensure that the statistical requirement is satisfied.

2.1 Scatter distribution from OFOV

A Philips GEMINI TF scanner was modeled in the simulation. It consists of 44 detector rings with 28 LYSO block detectors each. Each block was in a 23×44 array of 4 mm×4 mm×22 mm LYSO crystals with a 2.0 mm crystal pitch. The detector ring diameter is 90.34 cm, the length of AFOV is 18 cm and the diameter of the transverse field of view (TFOV) is 57.6 cm [16]. Simulations were performed with a short water-filled phantom (18 cm high and 20 cm in diameter) with a scattering medium in the field of view (FOV) only and a long water-filled phantom (36 cm high and 20 cm in diameter) with the same scattering medium within and external to the FOV. The long phantoms were twice the length of the short phantoms with the additional length added to both ends of the short phantom. A line source, which was 1.5 mm in radius and had the same length as each phantom, was positioned perpendicularly in the center of each phantom, respectively. Scatter contributions from the OFOV were acquired by subtracting the short phantom data from the long phantom data with the same activity density and data acquisition. OFOV SF refers to the counts of scatters from OFOV divided by the total counts without the scatters from OFOV. Both the radial and axial distributions of OFOV SF are shown here. Then the line source was moved 45 mm and 90 mm away from the center of the phantom and along the axis of the phantom to show the dependence of the scatter distribution from OFOV on the source position. Each phantom for each source position was scanned for 170 s to ensure that at least 10^9 coincidences are collected and then 3D data are reformed to 2D sinograms with the multi-slice rebinning algorithm. The OFOV SF values are plotted in the transverse and axial profile at each source position.

2.2 System-dependent application of scatter distribution from the OFOV

In order to characterize the scatters from OFOV in different PET systems, we chose four typical whole-

body and micro PET systems to examine the influence of scatters from OFOV with different scanner size. Therefore, except for the scanner size and structure, the other scanner parameters are the same. Here the Philips GEMINI TF, GE Discovery ST, Siemens Micro R4 Tomography and PET dedicated for breast cancer developed by the Institute of High Energy Physics (IHEP) and named as PEMi were simulated. The specifications of the four PET scanners are summarized in Table 1. A human-like IEC cylindrical phantom, a cylindrical phantom with three small cylindrical sources filled with water, polytetrafluoroethylene and air inserted was modeled. Detailed positions and sizes of the phantom are shown in Fig. 1. In each PET system 3D data were acquired for 30 sec and then reformed to 2D sinograms with the multi-slice rebinning algorithm. The OFOV SF values of each PET system were plotted in the axial profile and then OFOV SF as a function of ratio of ring diameter to length of AFOV was fitted.

Table 1. Scanner parameters of GEMINI TF, Discovery ST, R4 tomography and PEMi [16–19].

PET system	Philips GEMINI TF	GE Discovery ST	Siemens Micro PET R4 tomography	IHEP PEMi
crystal material	LYSO	LYSO	LYSO	LYSO
crystal size/mm^3	4×4×22	6.3×6.3×30	2.1×2.1×10	1.9×1.9×15
module array	23*44	12*24	8*32	16*64
ring num	44	24	32	64
module num	28	35	24	16
ring diameter/cm	90.34	88.6	14.8	16.6
transaxial FOV/cm	57.6	70	12.4	11.0
axial FOV/cm	18	15.7	7.8	12.8
ratio of ring diameter and AFOV	90.34/18=5.02	88.6/15.7=5.64	14.8/7.8=1.90	16.6/12.8=1.30

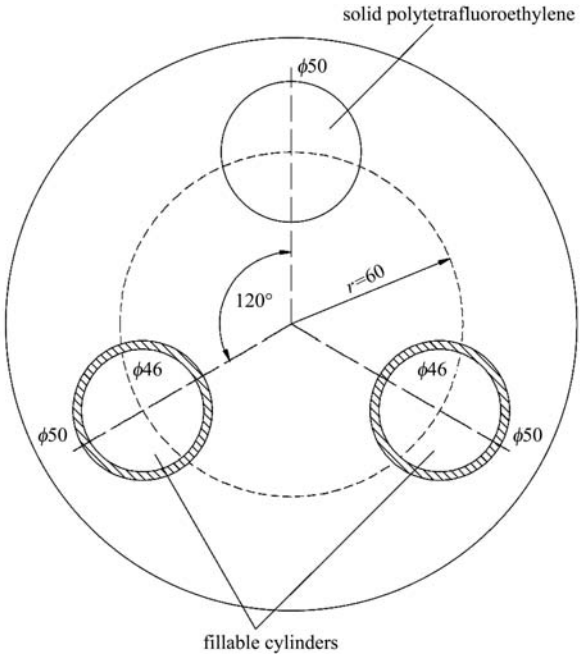

Fig. 1. Human-like IEC cylindrical phantom with three small cylindrical sources filled with water, polytetrafluoroethylene and air inserted [15].

2.3 Multiple scatter simulation

PET events are classified as true events (S_{0-0}), single scatter of one photon (S_{1-0}), single scatter of both photons (S_{1-1}), double scatter of one photon (S_{2-0}) and multi scatter ($S_{\rm m}$). Multiple SF refers to multiple scatter counts divided by the total counts including the true counts, single scatters and multiple scatters. In order to quantify the influence of multiple scatters between the whole-body PET and the micro PET, we modeled a water-filled phantom with a line source inserted in a Philips GEMINI TF. We also modeled a human-like IEC cylindrical phantom as Fig. 1 in four typical PET scanners and calculated their multiple SFs. The scatter and true events were directly obtained through the GATE "ASCII output". Therefore, the multiple SFs were computed from these raw outputs.

3 Result

3.1 Radial distribution of scatter from OFOV

OFOV SF is plotted against the radial position in Fig. 2. Outside the source, the OFOV SF value grows towards the edge of TFOV. It changes gently within the phantom and fluctuates sharply outside the phantom. The maximum radial OFOV SF is found when the line source is 90 mm off the center of phantom. Inside the source, the OFOV SF value drops down to approximately 0. That is, the scatters from OFOV tend to be recorded on the lines of response (LOR) far away from the source. The ax-

ial profiles of OFOV SF are showed in Fig. 3. These profiles are fitted with quadratic equations. The axial distributions of OFOV SF go up symmetrically from the center of AFOV to the ends. The maximum axial OFOV SF is found when the line source is 45 mm off the center of phantom.

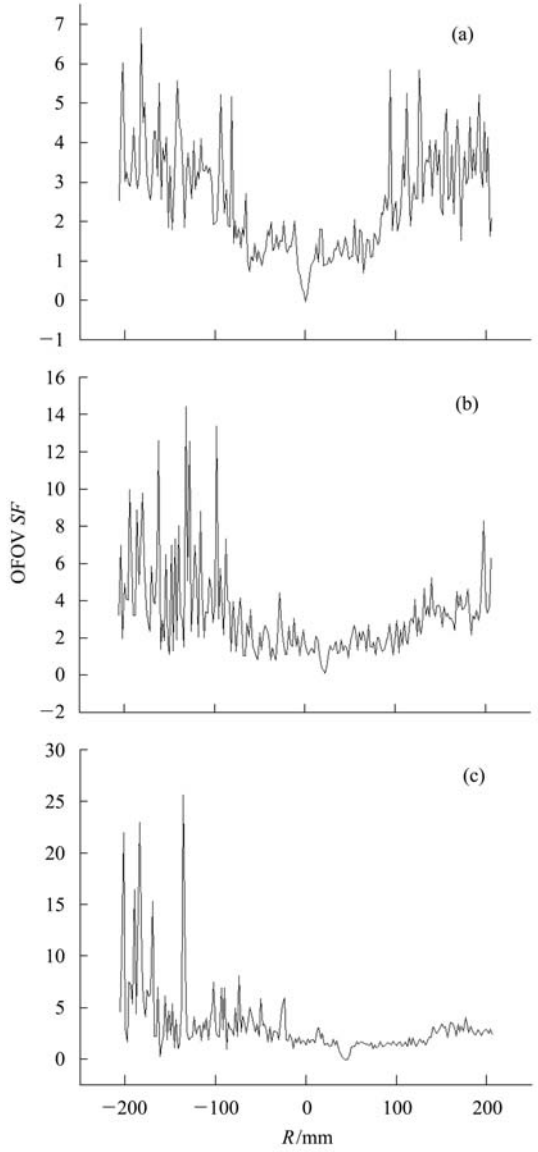

Fig. 2. The radial distribution of scatters from OFOV when the line source is located away from the center of the phantom: (a) 0 mm, (b) 45 mm and (c) 90 mm.

3.2 System-dependent application of scatter from OFOV

OFOV SFs are 1.3999, 1.4027, 0.1098 and 0.0479, respectively, in the Philips GEMINI TF, GE Discovery ST, Siemens Micro R4 tomography and PEMi. The maximum OFOV SF is found in the GE Discovery ST where the ratio of ring diameter to length of AFOV is larger than the other PET systems. A linear function can be used to fit the relation roughly between the OFOV SF and the ratio of scanner diameter to length of AFOV as showed in Fig. 4. The axial distributions of the OFOV SF of the four PET Systems are shown in Fig. 5. These profiles have similar distributions to quadratic equations.

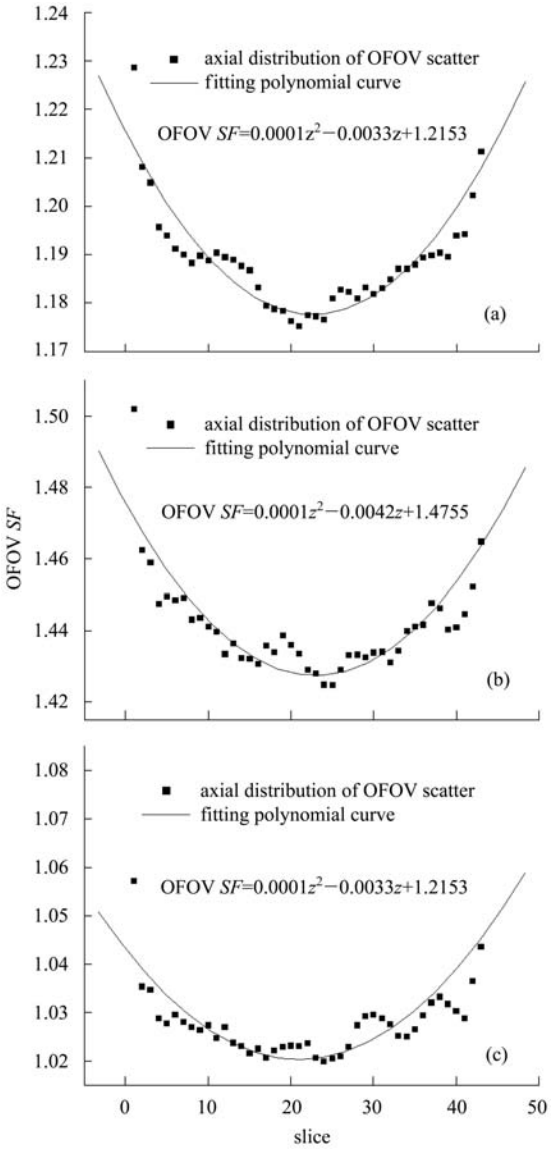

Fig. 3. The axial distribution of scatters from OFOV when the line source is located away from the center of the phantom: (a) 0 mm, (b) 45 mm and (c) 90 mm.

3.3 Multiple scatter simulation

In the Philips GEMINI TF system, multiple SFs of true events (S_{0-0}), single scatter of one photon (S_{1-0}), single scatter of both photons (S_{1-1}), double scatter of one photon (S_{2-0}) and multiple scatter (S_{m}) are 40.99%, 38.00%, 9.31%, 6.75% and 4.95% for the line source phantom simulation Table 2 lists

Table 2. Scatter fractions for GEMINI TF, Discovery ST, R4 tomography and PEMi.

multiple scatter fraction	Philips GEMINI TF	GE discovery ST	Siemens Micro PET R4 tomography	IHEP PEMi
S_{0-0}	53.59%	54.74%	90.37%	89.05%
S_{1-0}	33.42%	32.92%	9.02%	10.29%
S_{1-1}	5.16%	4.91%	0.20%	0.23%
S_{2-0}	5.24%	5.05%	0.37%	0.40%
S_{m}	2.60%	2.38%	0.04%	0.03%

multiple SFs of the human-like IEC cylindrical phantom simulation in the Philips GEMINI TF, GE Discovery ST, Siemens Micro R4 tomography and PEMi according to the system and the number of scatter interactions.

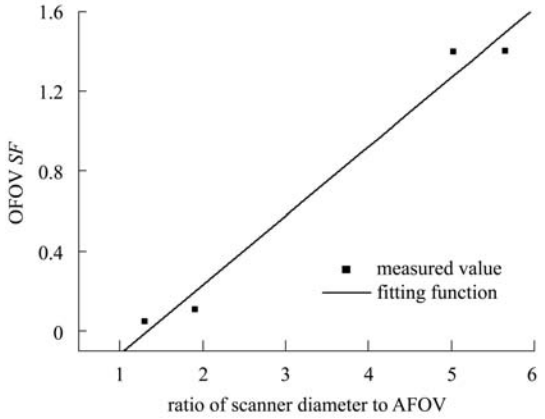

Fig. 4. OFOV SF as a linear function of ratio of scanner diameter to AFOV.

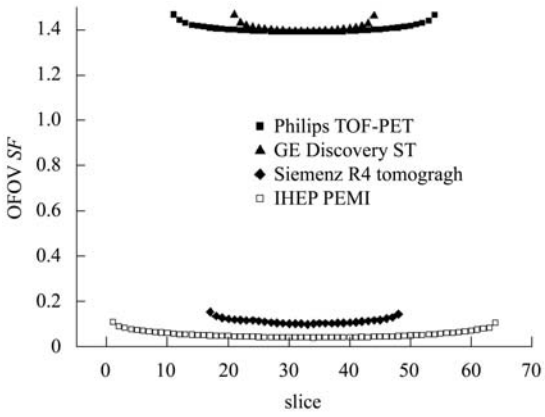

Fig. 5. The axial distributions of OFOV SF in TOF-PET, Discovery ST, R4 tomography and PEMi system.

4 Conclusion

In this work, the simulated investigation of the scatter from OFOV and multiple scatter was based on a series of protocols referring to those of the whole-body PET and the micro PET. The results show that there are a significant number of scatters from OFOV recorded on the LORs far away from the source, even outside the phantom. PET events recorded outside the phantom can be explained as scatter counts since true events must be collinear with the point of annihilation. These scatter contaminations may result from scatter coincidence from OFOV without the septa in 3D mode. The axial profile of OFOV SF is a parabolic curve because of the differences in axial sensitivity caused by the impact of material and activities from OFOV, which supports the result that axial scatter distribution from OFOV can be roughly fitted with a quadratic equation [6].

If we apply the above conclusion about the scatters from OFOV to different PET scanners, discrimination should be made between the whole-body PET and the micro PET. From Fig. 5 we can see that scatters from OFOV have a much less serious impact on the micro PET than on the whole-body PET depending on the scanner diameter and length of AFOV. The micro PET has a smaller scanner diameter than the whole-body PET and its gantry blocks the scatters from OFOV effectively. Additionally, PET with a longer AFOV length has a smaller OFOV SF because only a fraction of scatters with larger scatter angles from OFOV can be received by the detectors in deep slices. Therefore, in the whole-body PET, scatter from OFOV must be corrected for high quality image reconstruction, whereas in micro PET it can be ignored. As shown in Fig. 4, the relation between the OFOV SF (SF_{OFOV}) and the ratio (r) of scanner diameter to length of AFOV can be depicted with a linear function:

$$SF_{\mathrm{OFOV}} = 0.3467r - 0.4611.$$

From Table 2 we note that in the whole-body PET twice scatters, including single scatters of both photons S_{1-1} and double scatters of one photon S_{2-0}, add up to about 12% so that twice scatter correction must be implemented to remove them for high quality image reconstruction. Multiple scatters (scatters more than twice) should be eliminated because its proportion is small and its physical process is so complicated

that much more computing resources and time are consumed. In contrast, in micro PET, twice scatters occupy about 0.6% such that twice scatter correction should be ignored. These results support the conclusion that the amount of multiple scatter increases with the increasing object size [4]. In addition, we paid special attention to comparing single scatter of both photons and double scatter of one photon because they undergo twice scattering totally. Double scatter of one photon occupies comparable proportion with single scatter of both photons because the scattered photon is prone to scatter once again due to its loss of energy in the first scattering than the 511 keV unscattered photon [20]. Single scatter of both photons is differentiated from the multiple scatter of one photon because multiple scatter may drop much faster with a high energy window than the single scatter [6].When the energy window setting is high enough, multiple scatter can be ignored whereas the single scatter cannot.

In short, line source scattering phantom simulation shows that the scatters from OFOV tend to be recorded on the LORs far away from the source. Human-like IEC cylindrical phantom simulation indicates that the scatters from OFOV have a much more serious impact on the whole-body PET than the micro PET depending on the ratio of scanner diameter to length of AFOV. In the whole-body PET, twice scatters including single scatter of both photons (S_{1-1}) and double scatter of one photon (S_{2-0}) add up to about 12% so that twice scatter correction must be taken into account.

References

1 Lewellen T, Karp J. "PET systems" in Emission Tomography: The Fundamentals of PET and SPECT. San Diego, CA: Elsevier Academic Publishers, 2004. 190
2 Ollinger J M. Phys. Med. Biol., 1996, **41**: 153–176
3 Watson C C, Newport D, Casey M E, DeKemp R A et al. IEEE Trans. Nucl. Sci., 1997, **44**(1): 90–97
4 Adam L E, Karp J S, Brix G. Phys. Med. Biol., 1999, **44**: 2879–2895
5 Lewellen T K, Harrison R L, Kohlmyer S G. IEEE Trans. Nucl. Sci., 1999, **46**(4): 1129–1135
6 GAO F, Yamada R, Watanabe M, LIU H F. Chinese Physics B, 2009, **18**(7): 3066–3072
7 http://opengatecollaboration.healthgrid.org/
8 Jan S, Santin G, Strul D et al. Phys. Med. Biol., 2004, **49**: 4543–4561
9 Lazaro D, Buvat I, Loudos G et al. Phys. Med. Biol., 2004, **49**: 271–285
10 Schmidtlein C R, Kirov A S, Bidaut L M et al. Med. Phys., 2006, **33**: 198–208
11 Gonias P, Bertsekas N, Liaparinos P et al. Nucl. Instr. Meth. Phys. Res., 2007, **571**: 263–266
12 Santin G, Strul D, Lazaro D et al. IEEE Trans. Nucl. Sci., 2003, **50**: 1516–1521
13 Strul D, Santin G, Lazaro D et al. Nucl. Phys. B (Proc. Suppl.), 2003, **125**: 75–79
14 Rosslyn. VA: National Electrical Manufacturers Association, 2001. Standards Publication NU 2-2001
15 International Electrotechnical Commission, 1998. Publications IEC 60027
16 Vandenberghe S, Elmbt L V, Guerchaft M et al. Eur. J. Nucl. Med. Mol. Imaging, 2009, **36**: 1994–2001
17 Bettinardi V, Danna M, Savi A et al. Eur. J. Nucl. Med. Mol. Imaging, 2004, **31**: 867–881
18 Vandervoort E, Camborde M L, Jan S et al. Phys. Med. Biol. 2007, **52**: 3169–3184
19 YAN Qiang, GAO Juan, SHAN Bao-Ci, WEI Long. CPC (HEP & NP), 2010, **34**(1): 152–156
20 Markiewicz P J, Tamal M, Julyan P J et al. 2006 IEEE Nuclear Science Symposium Conference Record (IEEE Cat. No.06CH37832), 2007. 5